Cellulose(2014)21:4287-4298
DOI 10.1007/s10570-014-0411-3

ORIGINAL PAPER

Short cellulose nanofibrils as reinforcement in polyvinyl alcohol fiber

Jun Peng · Thomas Ellingham · Ron Sabo · Lih-Sheng Turng · Craig M. Clemons

Received 5 May 2014/Accepted 14 August 2014/Published online: 23 August 2014

Abstract Short cellulose nanofibrils (SCNF) were investigated as reinforcement for polyvinyl alcohol (PVA) fibers. SCNF were mechanically isolated from hard wood pulp after enzymatic pretreatment. Various levels of SCNF were added to an aqueous PVA solution, which was gel-spun into continuous fibers. The molecular orientation of PVA was affected by a combination of wet drawing during gel spinning and post-hot-drawing at a high temperature after drying. A maximum total draw ratio of 27 was achieved with various SCNF contents investigated. The PVA crystal orientation increased when small amounts of SCNF were added, but decreased again as the SCNF content was increased above about 2 or 3 %, likely due to SCNF percolation resulting in network formation that inhibited alignment. SCNF fillers were effective in improving PVA fiber tensile properties (i.e., ultimate strength and elastic modulus). For example, the ultimate strength and modulus of PVA/SCNF composite fiber with a SCNF weight ratio of 6 were nearly 60 and 220 % higher than that of neat PVA. Shifts in the Raman peak at ~ 1,095 cm^{-1}, which were associated with the C–O–C glycosidic bond of SCNF, indicated good stress-transfer between the SCNF and the PVA matrix due to strong interfacial hydrogen bonding. Cryogenic fractured scanning electron microscopy images of filled and unfilled PVA fibers showed uniform SCNF dispersion.

Keywords Short cellulose nanofibrils · Gel spinning · Polyvinyl alcohol · Nanocomposites · Stress transfer · Crystal orientation

J. Peng · T. Ellingham · L.-S. Turng (✉)
Polymer Engineering Center, University of Wisconsin–Madison, Madison, WI 53706, USA
e-mail:turng@engr.wisc.edu

J. Peng · T. Ellingham · L.-S. Turng
Wisconsin Institute for Discovery, University of Wisconsin–Madison, Madison, WI 53715, USA

R. Sabo · C. M. Clemons (✉)
Forest Products Laboratory, USDA Forest Service, Madison, WI 53726, USA
e-mail: cclemons@fs.fed.us

Introduction

Nanocellulose-based reinforcements constitute a new class of naturally-sourced reinforcements. Trees, plants, some marine creatures such as tunicates, and certain bacteria and algae form microfibrils from cellulose molecules. These microfibrils have a complex structural hierarchy and often act as the main reinforcing element in their respective organisms (Moon et al. 2011). In part, it is the high reinforcing potential of native crystalline cellulose within these microfibrils that has recently led researchers to extract nanocellulose from them for use in composites.

The mechanical properties of nanocellulose depend on its crystal structure, crystallinity, anisotropy,

defects, and isolation approaches (Moon et al. 2011). Several mechanical approaches, such as refining (Iwamoto et al. 2007), homogenizing (Zimmermann et al. 2010), cryocrushing (Dufresne et al. 1997), and high intensity ultrasonic treatment, have been employed to isolate cellulose fibrils from wood or plant fibers (Johnson et al. 2009). Cellulose nanofibrils (CNF) (also called nanofibrillated cellulose) are obtained by mechanical isolation, often after chemical or enzymatic pretreatment. CNF contains both amorphous and crystalline regions and typically have high aspect ratios (4–20 nm in width, 500–2,000 nm in length Moon et al. 2011). Cellulose nanocrystals (CNCs) are produced by acid hydrolysis, during which most of the amorphous fraction is removed. Depending on preparation and measurement methods, a tensile modulus of 10–35 GPa has been reported for CNF (Iwamoto et al. 2011; Sehaqui et al. 2012; Walther et al. 2011). The modulus of CNC would be expected to be much higher because of its highly crystalline nature. A Young's modulus of 138 GPa has been reported for native cellulose I crystals (Nishino et al. 1995).

However, some challenges exist to efficiently use nanocellulose as reinforcing fillers. For example, preparation of nanocellulose results in aqueous gels or suspensions that are not easily incorporated into most polymers. Also, nanocellulose is very hydrophilic, which can create difficulties in dispersing and bonding with many polymers. Water-soluble polymers are candidates for easy dispersion of nanocellulose and overcome these obstacles. Polyvinyl alcohol (PVA) is water-soluble, biodegradable, and biocompatible and has been broadly investigated for application including tissue scaffolding, filtration materials, membranes, and drug release (Nishiyama 1997). There has also been recent interest in using PVA fibers as a reinforcing fiber in cement in order to reduce bulk weight and improve strength (Sun et al. 2001; Zheng and Feldman 1995) or in woven or braided reinforcements for thermosetting or thermoplastic composites. PEO is also a water-soluble polymer in which CNC or CNF can achieve good dispersion (Xu et al. 2014). Compared with PEO as a polymeric matrix, PVA has much higher mechanical properties. To produce strong continuous fibers, PVA was focused on in this paper.

To improve the mechanical properties of PVA fibers, both CNC and CNF have been investigated as reinforcements. Uddin et al. (2011) produced gel-spun fibers from aqueous PVA solutions with up to 30 % CNC, followed by hot drawing. Adding 5 % CNC increased the ultimate tensile strength 20 % compared to neat PVA fibers. However, the tensile strength was reduced at concentrations above 5 % as PVA molecular orientation was reduced. Peresin et al. (2010) produced PVA mats with up to 15 % CNC by electrospinning and found that CNC increased the storage modulus. However, properties such as fiber strength or tenacity were not measured. Endo et al. gel-spun PVA that was reinforced with CNFs prepared using 2,2,6,6-tetramethylpiperidine-1-oxy radical (TEMPO)-mediated oxidation as a pretreatment prior to mechanical disintegration. They found the tensile strength did not improve with addition of 1 wt% CNF (Endo et al. 2013). A higher CNF content may have led to greater reinforcement. However, it was not possible to add more CNF due to the difficulty in dispersing the high aspect ratio CNF even with intense ultrasonication or strong mechanical stirring.

In this study, we investigated a new type of short cellulose nanofibers (SCNF) that are mechanically isolated from enzymatically pretreated wood pulp as reinforcement for the PVA fiber. Sufficient mechanical energy was used to prepare discrete CNF that could be used at higher weight percentages (compared to those reported previously) but without the need for concentrated sulfuric acid hydrolysis as in CNC production or the loss of hydroxyl groups for hydrogen bonding with the PVA matrix. Here, we investigated these SCNF in gel-spun PVA fibers.

Experiments

Preparation of short cellulose nanofibrils (SCNF)

SCNF was prepared at the U.S. Forest Service, Forest Products Laboratory (Madison, WI), according to the procedure described by previous paper (Qing et al. 2013; Zhu et al. 2011). A commercial hardwood bleached eucalyptus kraft pulp (Aracruz Cellulose, Brazil) was soaked in distilled water for 24 h before mechanical disintegrating in a blender for 10 min. The fiber slurry was then concentrated to 1.5 wt% pulp fiber by centrifuging. A commercial endoglucanase (Fibercare, Novozymes, Franklin, NC) was mixed with pulp fibers at 10 % solids and incubated at in a

Table 1 Compositions of PVA/SCNF spinning solutions and dry fiber

Sample	Weight (g)		Concentration (wt%)			SCNF/PVA ratio (%)
	20 wt% PVA solution	1 wt% SCNF suspension	Water	PVA	SCNF	
PVA	50	0	55	9	0	
PVA/SCNF1	50	10	51	9	0.09	1
PVA/SCNF2	50	20	41	9	0.18	2
PVA/SCNF3	50	30	31	9	0.27	3
PVA/SCNF6	50	60	1	9	0.54	6

flask on a shaker table at 50 °C for 24 h at 200 rpm. The enzymatically treated pulp fiber was then rinsed and fibrillated using a Super Mass Colloider (MKZA6-2, Masuko Sangyo Co, Japan). During fibrillation, the wet pulp fiber was fed between two-stone grinding disks with the gap of 100 micron and a rotation of 1,500 rpm. Approximately 100 g of pulp fibers (dry basis) were refined in circulation for 6 h. The suspension was further processed by running it fifteen times through a microfluidizer (M-110EH-30, Microfluidics, MA) with 200 and 87 μm chambers in sequence under a pressure of 150 MPa. The resulting SCNF suspension was stored in a cold room (4 °C) until used.

Preparation of spinning solution

A 99 % hydrolyzed commercial-grade of PVA from Sigma-Aldrich with a weight-average molecular weight of 85,000–124,000 was used as the matrix polymer. A sufficient amount of PVA was dissolved in water at 90 °C with mechanical stirring for 30 min to yield 20 % PVA by weight. Spinning solutions were prepared by mixing various amounts of SCNF solution, PVA solution, and water at 90 °C for 60 min. Specific compositions are listed in Table 1. The PVA/SCNF solutions were deaerated under vacuum at 90 °C for 10 min.

Fiber spinning and drawing

The PVA/SCNF dopes were spun into −20°C cold ethanol using a syringe pump and a 19 gauge needle (0.686 mm inner diameter) (Uddin et al. 2011). The needle tip was submerged about 1 mm into the ethanol. The spun wet fibers were collected by a rotating spool in the cold ethanol bath whose speed was set to yield a wet draw ratio of 2. The volumetric flow rate was 0.38 ml/min. The collected fibers were immersed in ethanol for 48 h followed by air drying for 24 h in a fume hood. Finally, the fibers were oven dried at 105 °C for at least 30 min. Dried fibers were preheated for 30 s in a hot tube at 210 °C and then manually drawn at 3-4 mm/s using a custom-designed clamping and drawing device. The total hot drawing process took <90 s, and the maximum hot draw ratio for all fibers was found to be about 13.5. This yielded a total draw ratio (wet and hot drawing) of 27 for all fibers. For comparison, a film of 100 % SCNF was also prepared for crystallinity (χ_c) measurements by casting a 1 wt% SCNF aqueous suspension into a petri dish followed by air drying.

Transmission electron microscopy (TEM)

The SCNF structure and dimensions were investigated by TEM. A few drops of diluted SCNF solution (0.5 wt% in water) were deposited on a TEM copper grid and dried. The sample grids were analyzed using a Philips CM-100 TEM (philips/FEI Corporation, Holland) at an accelerating voltage of 100 kV. ImageJ software (1.48d, developed by National Institutes of Health, US) was used to measure the length and diameter range based on the TEM images.

Scanning electron microscopy (SEM)

The outside surfaces and cryogenic and tensile fractured surface of PVA/SCNF filaments were analyzed by a scanning electron microscope (SEM; Model LEO 1530, JEOL, Japan) at an accelerating voltage of 3 kV.

Wide-angle X-ray diffraction (WAXD)

X-ray diffraction patterns were obtained with a Bruker Diffractometer (D8 Discovery, Bruker, US) by irradiating the PVA/SCNF fiber with Cu K*a* radiation

perpendicular to the fiber direction. The accelerating voltage and current were 50 kV and 1mA. PVA crystal orientation was determined using the most intense equatorial diffraction spots, those corresponding the (101/101) planes. Two approaches were employed to describe the crystal orientation: the degree of orientation (II) and Herman's orientation parameter (f) defined by Eqs. (1–3)(Ke 1964).

$$\Pi = \frac{180 - FWHM}{180} \quad (1)$$

$$f = \frac{3\langle cos^2\varphi\rangle - 1}{2} \quad (2)$$

$$\langle cos^2\varphi\rangle = \frac{\sum_0^{\pi/2} I(\varphi) sin\varphi cos^2\varphi}{\sum_0^{\pi/2} I(\varphi) sin\varphi} \quad (3)$$

where φ is the azimuthal angle and I(φ) is the intensity along the Debye–Scherrer ring. The value off ranges between −0.5 and 1 for perfect orientation perpendicular to and parallel to the fiber direction, respectively. Random orientation yields a value off of 0. The degree of orientation (II) formula estimates the orientation by the full width at half-maximum (FWHM) measurements of the peaks in a plot of intensity versus azimuthal angle at the relevant value of 20.

Segal's method was used to calculate the degree of crystallinity (χ_c) from the X-ray diffraction pattern using Eq. (4), where I_{200} is the intensity of the $(200)_{cell\ \ I\beta}$ (French 2013) or $(101)_{PVA}$ peak representing crystalline regions and I_{AM} is of the amorphous region (Segal et al. 1959; Seidel 2008),

$$\chi_c(\%) = \frac{I_{(200)cellI\beta\ or\ (101)PVA} - I_{AM}}{I_{(200)cellI\beta\ or\ (101)PVA}} * 100 \quad (4)$$

Tensile testing

Tensile properties were measured using a tensile testing machine (Instron, MA) with a 5 N load cell, a gauge length of 2.54 mm, and an extension rate of 0.254 mm/min following the ASTM D3379-75 standard (ASTM 1989). The diameter was measured by optical microscope and the fibers were conditioned at 25 °C and 50 % relative humidity prior to and during testing. The experimental results were evaluated as an average of 10 measurements. To ensure consistency and fair comparison, the composite fibers with the diameter of 45–55 μm (similar to those of pure PVA fibers) were selected via optical microscopy for tensile testing. As an approximation, a circular cross-section area was assumed for tensile properties calculation.

Molecular deformation studies using Raman spectroscopy

A Raman spectrometer (DXR, Thermo, US) coupled to an Olympus microscope was used to collect spectra from nanocomposite fibers during tensile deformation. The fiber was mounted on a commercial stretching stage with strain control. A 532 nm wavelength laser was focused on a spot size of 0.35 μm using the microscope with a 50× objective lens (numerical aperture of 0.75). Spectra were recorded using an exposure time of 100 s.

Results and discussion

Characterization of SCNF

An aqueous dispersion of SCNF was successfully prepared by enzymatic pretreatment and mechanical refining followed by 15 passes through a microfluidizer. The TEM image of dried 0.5 % SCNF solution shows discrete fibers of fairly low aspect ratio, (Fig. 1b), which is considerably different than the more networked structure typical of CNF (Fig. 1a) prior to microfluidizing. In fact, the SCNF looks similar to CNC in appearance (Moon et al. 2011; Wang et al. 2012). However, the surface properties are quite different. CNC are produced by sulfuric acid hydrolysis resulting in a sulfated surface. The SCNF were mechanically derived via microfluidizer from a CNF suspension, which had been previously enzymatically pretreated. The resulting SCNF has more available hydroxyl groups than the CNC, which improves the potential for hydrogen bonding with the PVA matrix, thus enabling enhanced mechanical performance. Image analysis yielded estimates of the length and diameter of 294 ± 95 and 13.6 ± 3.2 nm, respectively, and an aspect ratio of 15–28. To emphasize the different aspect ratio and surface groups of CNF, the term short cellulose nanofibrils (SCNF) is used here, not CNCs (Anderson et al. 2014; Mathew et al. 2014). Based on the XRD pattern of the 100 % cast SCNF film (Fig. 2), the crystallinity of the SCNF

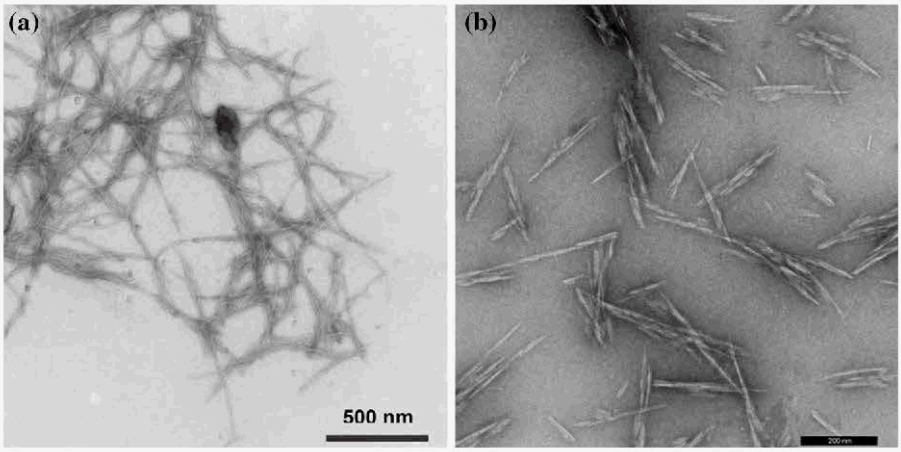

Fig. 1 TEM image of **a** CNF and **b** SCNF with the *scale bar* is 200 nm

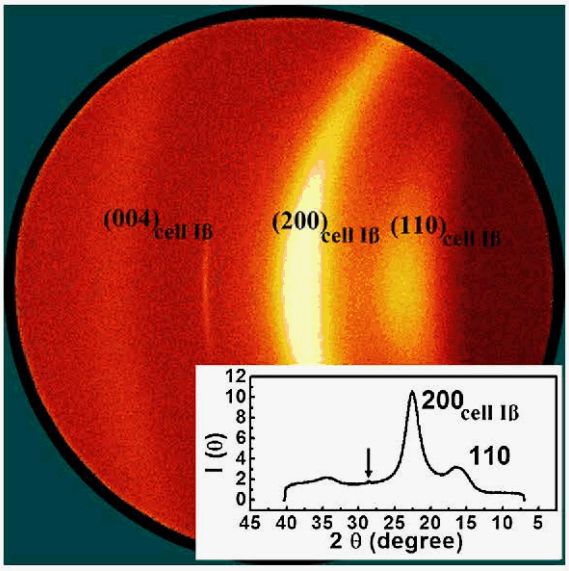

Fig. 2 WAXD pattern of pure SCNF cast film The *inset* is the intensity along the 2θ direction

was determined to be 80 %, as the same as the CNF before being processed by microfluidizer. This high crystallinity suggests high stiffness and a high reinforcing potential for the SCNF. Note that the narrow sharp peak halfway between the 200 and 004 intensities in Fig. 2 (indicated by the arrow) was likely due to Borax (sodium borate). Sodium borate, which has a strong 2 theta peak at 28.2 (Morris et al. 1981), was likely used as a fire retardant or an anti-fungal compound in the commercial pulp.

Fiber drawing

The SCNF/PVA weight ratio was varied from 1 to 6 %, since higher SCNF ratios caused unstable flow via gel spinning. Endo et al. reported that PVA fibers could not be spun by a similar gel spinning method if the CNF weight ratio was above 1 % in the PVA solution due to the difficulty in dispersing high aspect ratio CNF (Endo et al. 2013; Shinoda et al. 2012). The short aspect ratio of our SCNF made it possible to spin PVA solutions with more CNF and help to improve PVA fiber tensile properties.

Pure PVA fiber tensile properties and micromorphology depend greatly on chain extension and molecular orientation, which are largely controlled by drawing (Uddin et al. 2006, 2011). Since high temperature can increase molecular chain mobility as well as the reinforcing fillers' mobility in the polymeric matrix, hot drawing is a critical part of fiber manufacture, A temperature of 210 °C was used for hot drawing, which Endo et al. (2013) found optimal for similar composites. Fibers were exposed to 210 °C for <90 s to minimize possible thermal degradation. The consistently achievable maximum hot draw ratio (DR) for both pure PVA and filled PVA was 13.5, yielding a total draw ratio of 27, including the wet draw ratio of 2. Therefore, the addition of up to 6 % of SCNF did not limit the draw ratio of filled PVA fiber. This result is somewhat different than that found by Uddin et al. (2011) for CNC–PVA fibers. They found that adding 5 wt% CNC improved the drawability of PVA fiber and suggested that the CNC retarded

rupture during hot drawing. However, adding more than 5 % CNC decreased the maximum draw ratios proportional to the amount of CNC added.

According to Kanamoto et al. (1990), the critical minimum draw ratio (DR_{min}) for PVA for full molecular chain extension can be calculated by:

$$DR_{min} = 0.41 * (degree\ of\ polymerization)^{1/2} \quad (5)$$

The degree of polymerization of the PVA used in our investigation was about 2,000–2,800. Therefore, the DR_{min} for fully oriented PVA chains is about 18–21. Therefore, our maximum draw ratio of 27 suggests highly oriented PVA chains. XRD measurements (Table 2) showed that the crystallinity of the PVA fibers greatly increased during hot drawing, as is common for PVA fibers, due to bound water removal and increased molecular mobility and alignment during heat treatment. The degree of crystallinity depends on the temperature of the heat treatment; normally higher temperature leads to higher crystallinity (Lewin and Pearce 1998). PVA crystallinity decreased with the addition of SCNF (Table 2), which may have been the result of SCNF percolation and network formation. For rod-like nanoparticles, the percolation threshold (Φ_c) can be linked to the aspect ratio of the nanoparticles by the following equation (Siqueira et al. 2010):

$$\Phi_c = \frac{0.7}{L/d}. \quad (6)$$

In Eq. (6), L/d is the aspect ratio, which assumes a cylindrical shape. The calculated percolation threshold is about 2.5-4.9 %. When the SCNF weight ratio exceeds about 3 %, a network can form, which hinders chain mobility and, consequently, PVA crystallinity. The crystallinity of hot drawn PVA and composites fiber was a combination of stress induced crystallinity and thermally induced crystallinity. At high temperature, fiber drawing increases stress induced crystallinity as chains are aligned in the stretching direction. On the other hand, our drawing temperature of 210 °C might also result in thermally induced crystallinity. However, Wu et al. (2010) investigated various drawing rate and temperature effects on melt spun PVA fiber crystallinity, and found that the relatively low temperature of 210 °C did not affect the crystallinity since the temperature was not high enough to initiate chain relaxation. Therefore, the improved crystallinity of our hot drawn PVA and composite fibers results primarily from the stress induced crystallinity. In the next section, it will be shown that the crystallinity is closely related to orientation.

Crystal orientation analysis

Wide-angle X-ray diffraction (WAXD) was used to probe crystal orientation. Due to low SCNF filler concentrations, the diffraction patterns of SCNF crystals could not be discerned (Fig. 3). Concentric halos in Fig. 3a, b indicate random PVA (101/101) crystal orientation in wet drawn fibers, whether or not SCNF fibers were added. Equatorial spots in Fig. 3c, d from the (101/101) and (200) planes of PVA crystals indicated strong alignment in the hot drawn fibers.

Table 2 summarizes the degree of crystal orientation (II) and Herman's orientation parameter (f) from the overlapping diffraction peaks for the (101/101) planes of the PVA crystals. The orientation degrees (II) of all drawn fibers are similar. However, Herman's orientation parameters (f) were a more sensitive measure of PVA crystal orientation. Adding up to about 2–3% SCNF appeared to facilitate orientation, increasing the Herman's orientation parameter (f). That is, adding small amounts of SCNF filler appeared to facilitate orientation. At higher SCNF content, however, orientation was probably reduced because SCNF network formation hindered molecular alignment. Since crystallinity in our composites was primarily stress induced, it is not surprising that the crystallinity and crystal orientation values show the same trends (Table 2). Uddin et al. (2011) found a similar trend when CNC, rather than SCNF, was added to PVA. Adding small amounts of CNC increased orientation when drawing PVA fibers but higher CNC content (above 5 %)inhibited orientation. The authors also found CNC alignment as well. However, we could not measure the SCNF alignment at our somewhat lower levels of addition.

Tensile properties

Tensile tests were performed to quantify SCNF reinforcement of PVA fibers. Representative stress–strain curves are shown in Fig. 4, and the ultimate strength and Young's modulus of fiber with various SCNF ratios are summarized in Table 3. Adding

Table 2 Degree of crystal orientation (II), Hermans Orientation Parameter (f), and PVA crystallinity (χ_c) of single nanocomposites fibers

Samples	FWHM (°)	Orientation degree, II(%)	Herman's Parameter(f_c)	Crystallinity (χ_c)
Pure PVA[a]	N/A	N/A	N/A	20.7
Pure PVA[b]	5.8	96.8	0.65	64.4
PVA/SCNF1[b]	6.2	96.5	0.77	62.8
PVA/SCNF2[b]	6.4	96.4	0.80	63.0
PVA/SCNF3[b]	5.5	96.9	0.78	62.5
PVA/SCNF6[b]	5.9	96.7	0.63	58.9

[a] Wet draw ratio of 2

[b] Total draw ratio of 27 (wet draw ratio of 2 and hot draw ratio of 13.5)

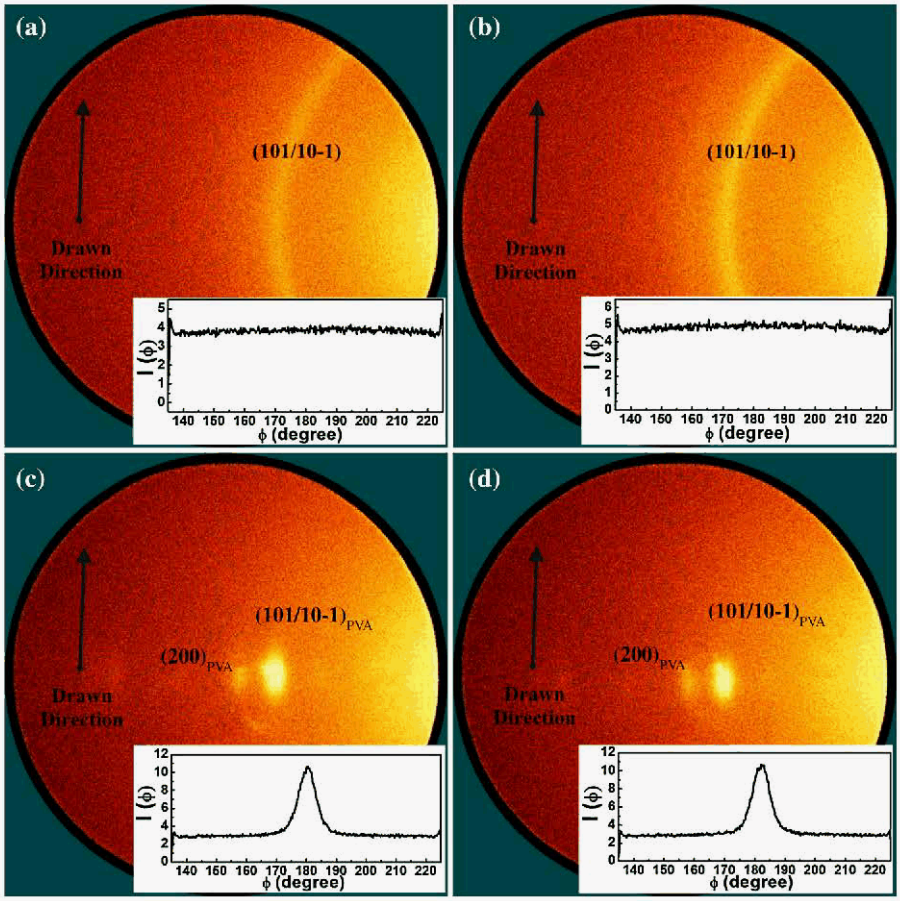

Fig. 3 Two dimensional WAXD patterns of **a** wet drawn and **c** wet and hot drawn pure PVA fiber, and **b** wet drawn and **d** wet and hot drawn PVA/SCNF3. The *insets* are the Azimuthal intensity distributions of the equatorial reflection PVA crystal (101/10-1)

SCNF to PVA generally yielded stronger, stiffer, and even tougher fibers. The ultimate strength of the PVA/SCNF fibers are related to both PVA crystal orientation and the amount of SCNF added (Fig. 5), but SCNF loading governs the strength. The tensile moduli of filled PVA fibers increased proportionally with the addition of SCNF. However, the ultimate strength peaked at a PVA: SCNF weight ratio of about 3 %. Below the percolation threshold (likely around 2.5-4.9 % SCNF), the strength increased due to the addition of SCNF as well as the increased PVA matrix crystal orientation. At higher loadings, gains in

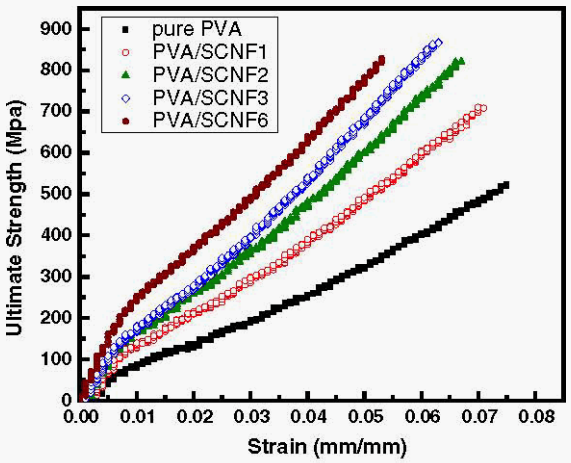

Fig. 4 Stress–strain curves of the pure PVA and PVA/SCNF nanocomposite fibers

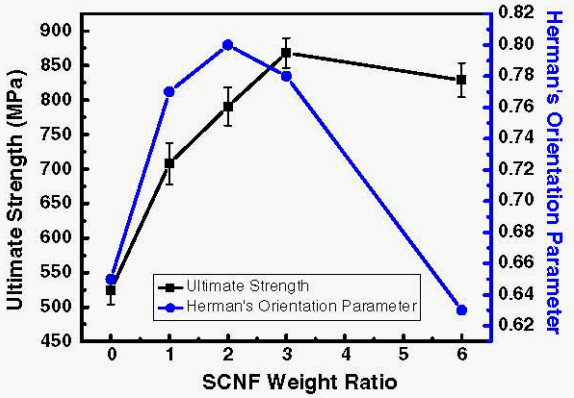

Fig. 5 Comparisons of SCNF weight ratios and crystal orientation effects on ultimate fiber strength

Table 3 Tensile properties of pure PVA and PVA/SCNF fibers

Samples	Ultimate strength (MPa)	Young's modulus (GPa)	Toughness (MPa)
Pure PVA	524.6 ± 21.0	10.1 ± 0.4	18.9 ± 1.3
PVA/SCNF1	707.7 ± 29.7	14.6 ± 0.6	25.1 ± 2.2
PVA/SCNF2	790.6 ± 27.7	20.6 ± 0.7	27.6 ± 1.9
PVA/SCNF3	868.3 ± 21.7	21.6 ± 0.5	27.3 ± 2.3
PVA/SCNF6	828.8 ± 24.9	32.3 ± 1.0	23.7 ± 3.2

strength were largely maintained despite reductions in PVA orientation due to increased reinforcement from the additional SCNF (Table 2; Fig. 5). Despite the drawn pure PVA and PVA/SCNF6 composite having comparable Herman's orientation parameter values, the ultimate strength and modulus of PVA/SCNF6 were nearly 60 and 220 % higher than that of neat PVA.

Moisture sorption can have a large influence on the mechanical performance of PVA. Heat treatment helps to mitigate this moisture sensitivity by removing residual water, resulting in the formation of new hydrogen bonds and increased crystallization (Lewin and Pearce 1998). Due to the elevated temperature during drawing (210 °C), our fibers would be expected to undergo heat treatment as well strain induced crystallization due to the high draw ratios used. Nevertheless, remaining moisture sensitivity is possible, especially considering limitations on the fiber drawing temperature due to the limited thermal stability of the SCNF as well as the moisture sensitivity of the SCNF itself. This is a current avenue of exploration and need further investigation.

Raman spectroscopy and stress-transfer mechanism in composites

Cellulose has a well-defined Raman band at 1,095 cm^{-1}, which is associated with C–O–C glycosidic bond stretching (Gierlinger et al. 2006; Sturcova et al. 2005; Wiley and Atalla 1987). This band has been shown to shift under strain as the change in stress state influences bond deformation. These shifts have been used to investigate stress transfer in cellulose nano-whisker reinforced epoxies, for example (Rusli et al. 2010). In the present study, this technique was applied to the PVA and PVA/SCNF fibers.

Figure 6 shows typical Raman spectra for pure SCNF cast film, as well as pure PVA and PVA/SCNF3 drawn filaments. When the SCNF:PVA weight ratio was more than 3 %, the characteristic cellulose peak at 1,095 cm^{-1} could be discerned. PVA also had a small peak at ~1,095 cm^{-1} due to the C–O out of plane bending vibration (Deepak et al. 2012). However, little or no shift in this peak was found when the pure PVA fiber was strained (Fig. 7). This may be because this peak involved the bending of the hydroxyl side groups rather than the stretching of the primary bonds in the polymer backbone, as is the case in the cellulose in SCNF. Therefore, the shift in the cellulose 1,095 cm^{-1} band for PVA/SCNF under strain may not be affected

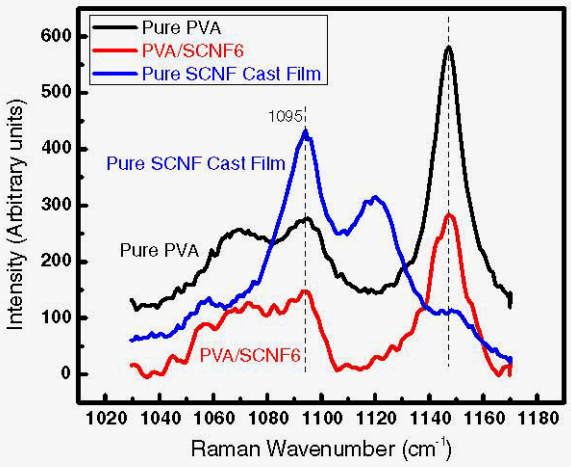

Fig. 6 Typical Raman spectra for pure SCNF cast film, pure PVA and PVA/SCNF3 drawn filaments highlighting the Raman peak initially located at ~ 1,095 cm^{1}

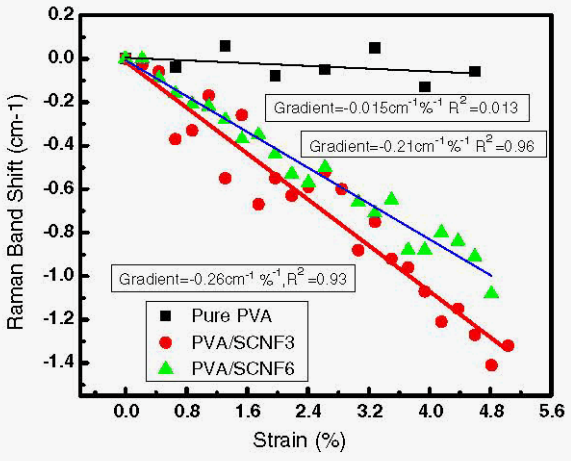

Fig. 7 Shifts in the Raman band position initially located at −1,095 cm^{-1} upon tensile deformation for pure PVA, PVA/SCNF3, and PVA/SCNF6 drawn fiber with a draw ratio of 27. *Solid lines* are linear regressions for the data

by the PVA band at that position, unless the addition of nanocellulose results in a new deformation mechanism involving the PVA hydroxyl side chains.

Figure 7 shows typical 1,095 cm^{-1} band shifts when the PVA/SCNF3 and PVA/SCNF6 fibers are strained. This shift suggests stress transfer through the hydrogen bonds between SCNF and PVA matrix, or between the SCNF themselves due to percolation, or both. The rates of the band shifts with strain (Fig. 7) were −0.26 and −0.21 $cm^{-1}\%^{-1}$ for PVA/SCNF3 and PVA/SCNF6 hot drawn fibers, respectively. The lower rate for the composite fiber with more SCNF may be related its lower crystal orientation and resulting reduced stress transfer ability in the fiber direction. Prior to fracture, there was no discontinuity or change in the slope of the curves in Fig. 7 for the composite fibers that would suggest SCNF–PVA debonding. This further indicates strong filler-matrix adhesion due to hydrogen bonding (Rusli et al. 2011).

Cryogenic fracture morphologies

The outside surfaces of the pure and filled PVA fibers are shown in Fig. 8. The pure PVA fibers possess a smooth and homogeneous surface, while PVA/SCNF has an irregular surface. Such irregular surfaces are common in the PVA fibers and result from a faster rate of water diffusion out of the fiber than the coagulant diffusion into the fiber after the skin is formed (Elices and Llorca 2002). The relative diffusion rates are likely affected by the SCNF. Some SCNF tips appear on the outside surface of PVA/SCNF6 fiber, as shown in Fig. 8d.

Figure 9 presents the cryogenically fractured cross sections of pure and filled PVA fibers. The cross–sections are approximately circular and have diameters ranging from 45 to 55 μm. Compared to pure PVA, filled PVA fibers were more variable in diameter. Figure 9b is an enlarged image of the cross-section of the pure PVA fiber showing a smooth surface. A comparable image for the PVA/SCNF3 fiber (Fig. 9d) shows a much rougher fracture surface and less than perfect SCNF dispersion. PVA/SCNF3 cross-section features are shown since it had the maximum ultimate strength and had similar SCNF dispersion features as that of PVA/SCNF6.

Conclusions

Discrete, highly crystalline SCNF can be produced from enzymatically pretreated cellulose when sufficient mechanical energy is applied. These SCNF are similar in appearance to CNCs but do not require concentrated sulfuric acid (typically more than 60 % v/v) for their preparation. Reducing the energy requirement through optimization of the enzymatic pretreatment could reduce cost and the environmental footprint as well. The greater

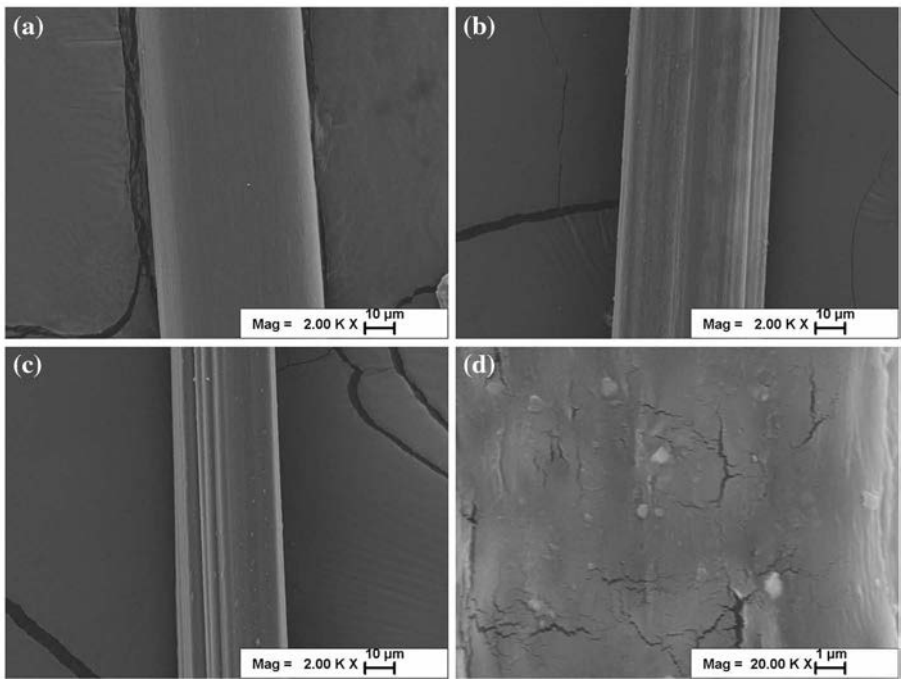

Fig. 8 SEM images of **a** pure PVA, **b** PVA/SCNF3, **c** PVA/SCNF6 and **d** enlarged image **(c)** fiber with a total draw ratio of 27

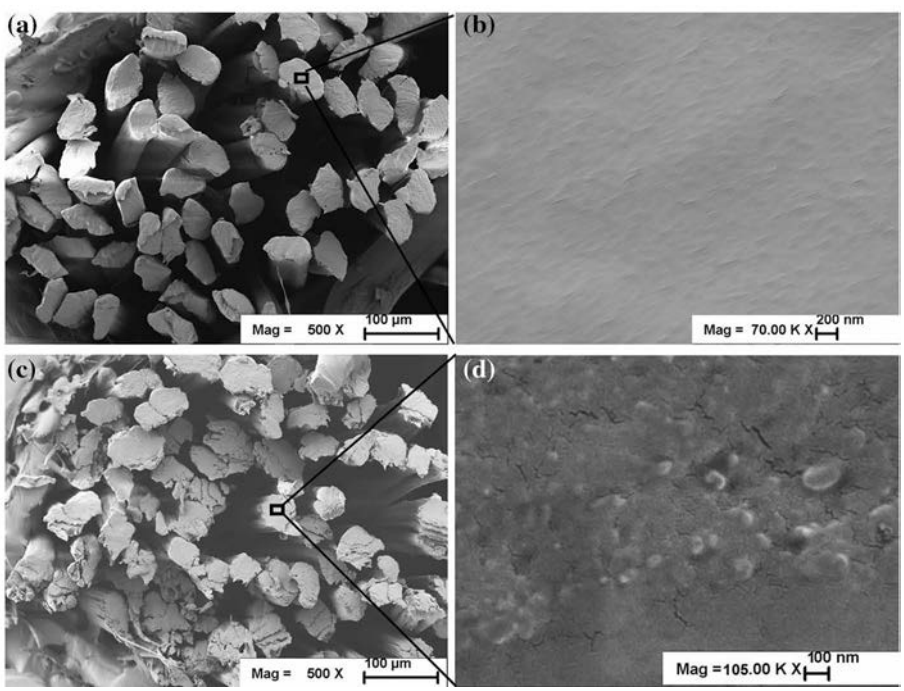

Fig. 9 SEM images of the cryogenic fracture surfaces for **a** the pure PVA fibers, **b** the pure PVA fibers at a larger magnification, **c** PVA/SCNF3 fiber, and **d** PVA/SCNF3 fiber at a larger magnification

number of hydroxyl groups compared to cellulose fibrils may also offer some advantages as reinforcement for polymers like PVA.

Adding small amounts (<3 %) increased the orientation of the crystalline PVA fraction at the same maximum draw ratio of 27. However, further addition of SCNF began to reduce the orientation possibly as a result of SCNF network formation that limited molecular alignment. Raman C–O-C glycosidic peak shift rates under uniaxial strain indicated good stress transfer between the SCNF and the PVA matrix. Improvements in tensile strength appeared to be due to a combination of increased orientation (at low SCNF weight ratios) and SCNF reinforcement. Further increases in tensile strength as SCNF levels approaching 6 % were prevented by reductions in orientation and crystallinity. However, modulus increases with SCNF content over the entire SCNF range investigated. Cryogenically fractured fiber indicated SCNF were less than perfectly dispersed at the magnifications investigated but further work is warranted. Initial evaluation of SCNFs as reinforcing fibers appears promising, particularly at low levels of addition, but further work is necessary to understand, predict, and optimize SCNF reinforcement.

Acknowledgments This project was supported by the USDA National Institute of Food and Agriculture Award (No. 2011-67009-20056). The authors would like to acknowledge Yan Qing and J.Y. Zhu for processing the short cellulose nanofibrils. Debby Sherman at Purdue University is kindly acknowledged for TEM imaging. The first author also wishes to acknowledge the National Nature Science Foundation of China (Nos. 51073601, 21174044), the Fundamental Research Funds for the Central Universities (No. 2011220011), the China Postdoctoral Science Foundation (2012M511791), and the 973 Program (2012CB025902) for their financial support.

References

Anderson SR, Esposito D, Gillette W, Zhu JY, Baxa U, McNeil SE (2014) Enzymatic preparation of nanocrystalline and microcrystalline cellulose. TAPPIJ 13:35-41

ASTM (1989) Standard test method for tensile strength and Young's modulus for high-modulus single-filament materials vol D3379-75

Deepak KLN, Rao DN, Rao V (2012) Spectroscopic investigation of fs laser-induced defects in polymer and crystal media. In: Proceedings of the SPIE 8530, laser-induced damage in optical materials, December 4, 2012. doi:10.1117112.975812

Dufresne A, Cavaille JY, Vignon MR (1997) Mechanical behavior of sheets prepared from sugar beet cellulose microfibrils. J Appl Polym Sci 64:1185–1194

Elices M, Llorca J (2002) Fiber fracture. Elsevier Science Ltd, Kidlington

Endo R, Saito T, Isogai A (2013) TEMPO-oxidized cellulose nanofibril/poly(vinyl alcohol) composite drawn fibers. Polymer 54:935–941.doi:10.1016/j.polymer.2012.12.035

French AD (2013) Idealized powder diffraction patterns for cellulosepolymorphs. Cellulose 21:885–896doi:10.10071s10570-013-0030-4

Gierlinger N, Schwanninger M, Reinecke A, Burgert I (2006) Molecular changes during tensile deformation of single wood fibers followed by Raman microscopy. Biomacromolecules 7:2077–2081

Iwamoto S, Nakagaito AN, Yano H (2007) Nano-fibrillation of pulp fibers for the processing of transparent nanocomposites. Appl Phys A 89:461-466

Iwamoto S, Isogai A, Iwata T (2011) Structure and mechanical properties of wet-spun fibers made from natural cellulose nanofibers.Biomacromolecules 12:831-836.doi:10.10211bm101510r

Johnson R K , Zink-Sharp A, Renneckar SH, Glasser WG (2009) A new bio-based nanocomposite: fibrillated TEMPO-oxidized celluloses in hydroxypropylcellulose matrix. Cellulose 16:227–238

Kanamoto T, Kiyooka S, Tovmasyan Y, Sano H, Narukawa H (1990) Effect of molecular-weight on drawing poly(vinyl alcohol) from solution-grown crystal mats. Polymer 31:2039–2046. doi:10.1016/0032-3861(90)90073-8

Ke B (1964) Newer methods of polymer characterization, vol 6. Interscience Publishers, New York, NY

Lewin M, Pearce EM (1998) Handbook of fiber chemistry, 2nd edn. Marcel Dekker Inc., Brookly, NY

Mathew AP, Oksman K, Karim Z, Liu P, Khan SA, Naseri N (2014) Process scale up and characterization of wood cellulose nanocrystals hydrolysed using bioethanol pilot plant. Ind Crops Prod 58:212–219.doi: 10.1016/j.indcrop.2014.04.035

Moon RJ, Martini A, Nairn J, Simonsen J, Youngblood J (2011) Cellulose nanomaterials review: structure, properties and nanocomposites. Chem Soc Rev 40:3941–3994. doi: 10.1039/c0cs00108b

Morris MC, McMurdie HF, Evans EH, Paretzkin B, Parker HS, Panagiotopoulos NC (1981) Standard X-ray diffraction powder patterns: section 18. Data for 58 substances. National Bureau of Standards, Washington, DC

Nishino T, Takano K, Nakamae K (1995) Elastic-modulus of the crystalline regions of cellulose polymorphs. J Polym Sci Polym Phys 33:1647–1651

Nishiyama M (1997) New synthetic fiber and its applications. Chem Fibers Int 47:296–297

Peresin MS, Habibi Y, Zoppe JO, Pawlak JJ, Rojas OJ (2010) Nanofiber composites of polyvinyl alcohol and cellulose nanocrystals: manufacture and characterization. Biomacromolecules 11:674–681

Qing Y, Sabo R, Zhu JY, Agarwal U, Cai Z, Wu Y (2013) A comparative study of cellulose nanofibrils disintegrated via multiple processing approaches. Carbohydr Polym 97:226–234. doi:10.1016/j.carbpo1.2013.04.086

Rusli R, Shanmuganathan K, Rowan SJ, Weder C, Eichhorn SJ (2010) Stress-transfer in anisotropic and environmentally adaptive cellulose whisker nanocomposites. Biomacromolecules 11:762–768

Rusli R Shanmuganathan K, Rowan SJ, Weder C, Eichhorn SJ (201 1) Stress transfer in cellulose nanowhisker composites—influence of whisker aspect ratio and surface charge. Biomacromolecules 12:1363–1369. doi:10.1021/bm200141x

Segal L, Creely JJ, Martin AE, Conrad CM (1959) An empirical method for estimating the degree of crystallinity of native cellulose using the X-ray diffractometer. Text Res J 29:786. doi:10.1177/004051755902901003

Sehaqui H, Ezekiel Mushi N, Morimune S, Salajkova M, Nishino T, Berglund LA (2012) Cellulose nanofiber orientation in nanopaper and nanocomposites by cold drawing. ACS Appl Mater Interfaces 4:1043–1049. doi:10.1021/am2016766

Seidel A (2008) Characterization and analysis of polymers, 1st edn. Wiley-Interscience, Hoboken, NJ

Shinoda R, Saito T, Okita Y, Isogai A (2012) Relationship between length and degree of polymerization of TEMPO-oxidized cellulose nanofibrils. Biomacromolecules 13:842-849. doi:10.l021/Bm2017542

Siqueira G, Bras J, Dufresne A (2010) Cellulosic bionanocomposites: a review of preparation, properties and applications. Polymers 2:728–765

Sturcova A, Davies GR, Eichhorn SJ (2005) Elastic modulus and stress-transfer properties of tunicate cellulose whiskers. Biomacromolecules 6:1055–1061

Sun W, Chen HS, Luo X, Qian HP (2001) The effect of hybrid fibers and expansive agent on the shrinkage and permeability of high-performance concrete. Cem Concr Res 31:595-601

Uddin AJ, Ohkoshi Y, Gotoh Y, Nagura M, Endo R, Hara T (2006) Effects of take-up speed of melt spinning on the structure and mechanical properties of maximally laser drawn Pa9-T fibers. Int Polym Process 21:263–271

Uddin A, Araki J, Gotoh Y (2011) Toward "strong" green nanocomposites: polyvinyl alcohol reinforced with extremely oriented cellulose whiskers. Biomacromolecules 12:617–624. doi:10.1021/bm101280f

Walther A Timonen JV, Diez I, Laukkanen A, Ikkala O (2011) Multifunctional high-performance biofibers based on wet-extrusion of renewable native cellulose nanofibrils. Adv Mater 23:2924–2928. doi:10.1002/adma.201100580

Wang QQ, Zhu JY, Reiner RS, Verrill SP, Baxa U, McNeil SE (2012) Approaching zero cellulose loss in cellulose nanocrystal (CNC) production: recovery and characterization of cellulosic solid residues (CSR) and CNC. Cellulose 19:2033–2047. doi:10.1007/s10570-012-9765-6

Wiley JH, Atalla RH (1987) Band assignments in the Raman-spectra of celluloses. Carbohydr Res 160:113–129

Wu QA, Chen N, Wang Q (2010) Crystallization behavior of melt-spun poly(vinyl alcohol) fibers during drawing process. J Polym Res 17:903–909

Xu XZ, Wang HR, Jiang L, Wang XN, Payne SA, Zhu JY, Li RP (2014) Comparison between cellulose nanocrystal and cellulose nanofibril reinforced poly(ethylene oxide) nanofibers and their novel shish-kebab-like crystalline structures. Macromolecules 47:3409–3416

Zheng ZH, Feldman D (1995) Synthetic fiber-reinforced concrete. Prog Polym Sci 20:185–210

Zhu JY, Sabo R Luo X (2011) Integrated production of nano-fibrillated cellulose and cellulosic biofuel (ethanol) by enzymatic fractionation of wood fibers. Green Chem 13:1339. doi:10.1039/c1gc15103g

Zimmermann T, Bordeanu N, Strub E (2010) Properties of nanofibrillated cellulose from different raw materials and its reinforcement potential. Carbohydr Polym 79:1086-1093. doi:10.1016/j.carbpol.2009.10.045